JACS Au
AN OPEN ACCESS JOURNAL OF THE AMERICAN CHEMICAL SOCIETY

pubs.acs.org/jacsau
Article

Efficient Biomimetic Total Synthesis, Characterization, and Antioxidant Activity of Ommatins

Lili Huang, Taehwan Kim, Olivia J. Armendarez, Leila F. Deravi, Prakash T. Parvatkar,* and Roman Manetsch*

Cite This: JACS Au 2024, 4, 4307−4316
Read Online
ACCESS | Metrics & More | Article Recommendations | Supporting Information

ABSTRACT: Ommatins, natural colorants found in cephalopods and arthropods, are biosynthesized from tryptophan with uncyclized xanthommatin (Uc-Xa) as the key biosynthetic precursor. These pigments change color under oxidative or reductive conditions. Xanthommatin (Xa) and dihydro-xanthommatin (H_2-Xa), as well as decarboxylated xanthommatin (Dc-Xa) and decarboxylated-dihydro-xanthommatin (Dc-H_2-Xa), are some of the most common and well-studied ommatins. Herein, we describe the biomimetic total synthesis of Xa/H_2-Xa on a gram scale by using the Mannich reaction and oxidative dimerization as the key steps. The 7-step linear synthetic sequence achieved an overall yield of 27%. Dc-Xa/Dc-H_2-Xa and protected Uc-Xa/Uc-H_2-Xa were also synthesized from the common intermediate-protected 3-hydroxykynurenine (3-OHK). The synthesized ommatins underwent thorough characterization using various spectroscopic techniques, including NMR, UV−vis, FTIR, HRMS, and LC−MS. Their optoelectronic properties were studied using spectrophotometry and electrochemical analysis. Furthermore, the antioxidant activity of the synthesized ommatins was evaluated using an oxygen radical antioxidant capacity activity assay. The results indicated that Dc-Xa exhibited the highest antioxidant activity, followed by Xa, while Uc-Xa showed the lowest activity.

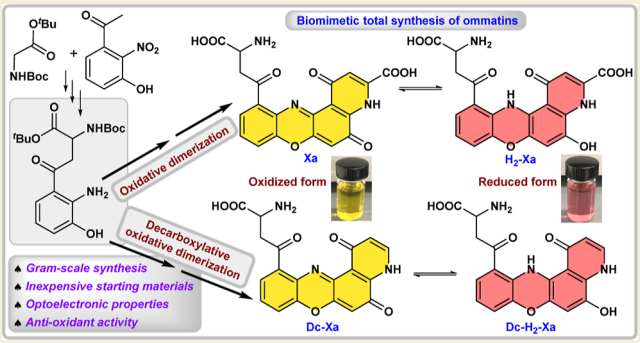

KEYWORDS: *antioxidant, natural product, ommochrome, optoelectronic, oxidative cyclization, phenoxazinone, xanthommatin*

INTRODUCTION

Ommochromes are natural pigments found in invertebrate animals, including cephalopods.[1−3] They are known for their ability to mediate color, with colors ranging from pale yellow to deep purple.[4] Ommochromes play a role in crypsis, mimicry, sexual maturation, and many other color-based functions.[4] They are believed to provide light shielding and antioxidant protection to photoreceptor cells, control over spectral sensitivity, skin coloration, and detoxification of excess tryptophan.[2] In addition, ommochromes have been used as a scaffold for designing antitumor agents[5] and biomimetic electrochromic devices.[6]

Becker initiated the early studies of ommochromes from insect ommatidia (from which their name was derived) in the 1930s,[7,8] and later, Butenandt's group delved into their chemistry and biogenetic pathway.[1] Due to their challenging nature, ommochromes are difficult to study.[9−12] This is mainly because they are typically available in small quantities and do not readily dissolve in solvents. Moreover, they tend to aggregate and undergo reversible and nonreversible transformations that require fast processing. The chemical structure of ommochromes has been precisely proposed for only a few, primarily through mass spectrometry. Two prominent families of natural ommochromes are yellow-to-red ommatins and purple ommins (Figure 1).[13] Ommatins contain a phenoxazinone ring, have low molecular weight, and are thermolabile (e.g., xanthommatin).[14] They are the more extensively studied family and are found throughout invertebrates. Ommins, on the other hand, contain an additional phenothiazine ring, have high molecular weight, and are thermoresistant (e.g., ommin A, the structure remains speculative). Although ommins are present in insects and cephalopods, they are not well characterized.[10,15]

Xanthommatin (Xa) is one of the most well-studied ommochromes whose structure was elucidated by Butenandt in 1954.[16] It belongs to the ommatin family and appears yellow in its oxidized form. However, it turns red when reduced to dihydro-xanthommatin (H_2-Xa). This unusual color-changing molecular property is responsible for critical biological

Received: July 23, 2024
Revised: October 12, 2024
Accepted: October 14, 2024
Published: October 23, 2024

https://doi.org/10.1021/jacsau.4c00667
JACS Au 2024, 4, 4307−4316

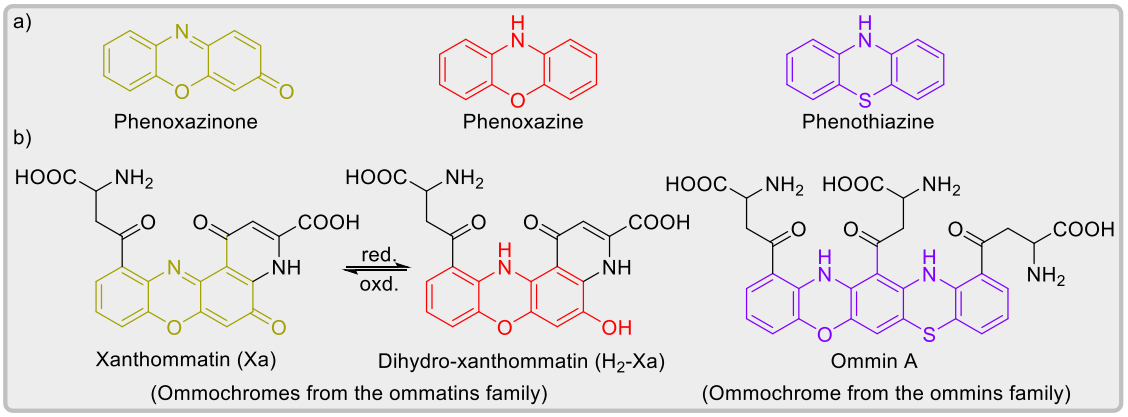

Figure 1. (a) Chemical structures of phenoxazinone, phenoxazine, and phenothiazine. (b) Representative examples of natural ommochromes.

Scheme 1. Reported Proposed Biosynthetic Pathway of Ommatins[4,12,13a]

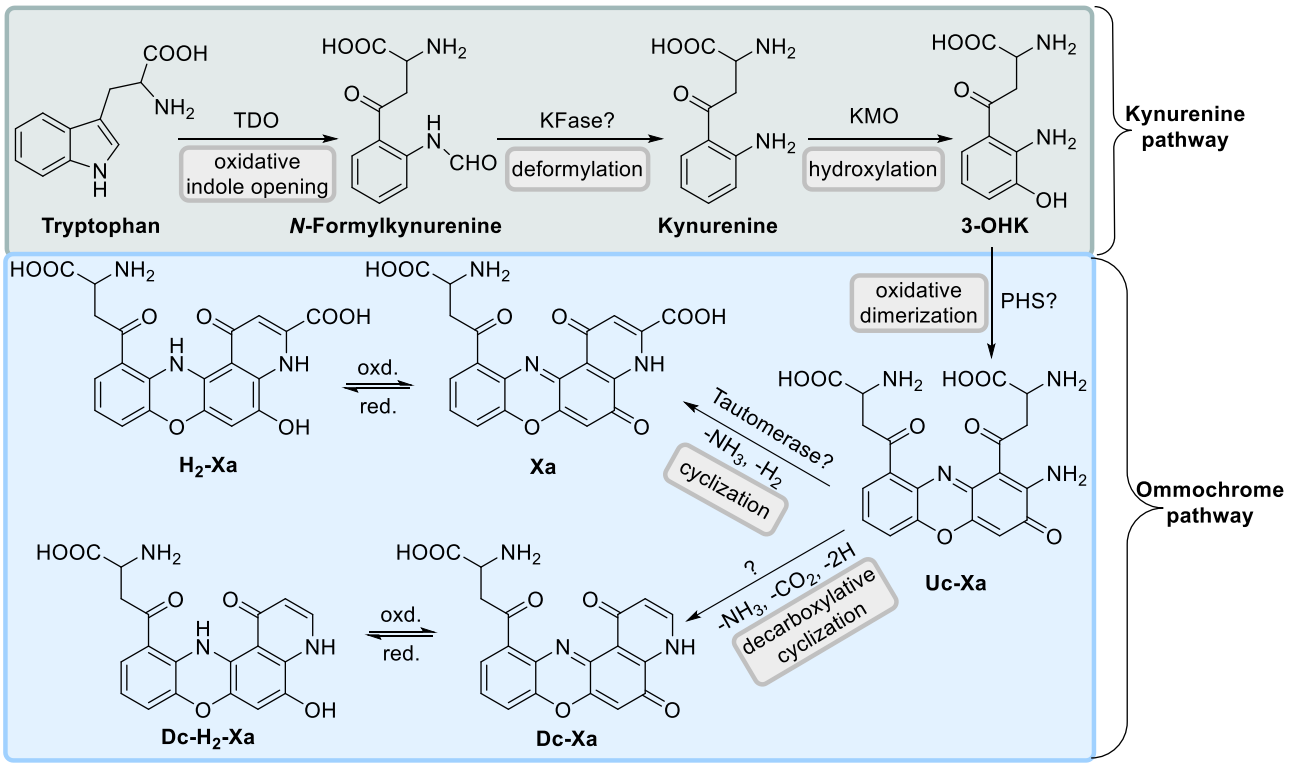

[a]TDO—tryptophan 2,3-dioxygenase, KFase—kynurenine formamidase, KMO—kynurenine 3-monooxygenase, PHS—phenoxazinone synthase, oxd.—oxidation, and red.—reduction.

functions such as nuptial colorations in dragonflies,[17] light filtering in insect eyes,[18] and electron transfer in various insects and marine worms.[19−22] Additionally, the bathochromic reduction of Xa has shown potential for crafting color-changing electrochromic devices.[6] Recently, decarboxylated xanthommatin (Dc-Xa) and dihydro-xanthommatin (H_2-Xa) have been identified.[13] They were first discovered in the in vitro oxidation of ommochrome precursors but were subsequently found in extracts of crab spiders, dragonflies, silkworms, and cephalopods.[4]

The reported plausible biosynthetic pathway of ommatins is shown in Scheme 1.[4,12,13] The early stages of ommatin biosynthesis in invertebrates involve the conversion of tryptophan into 3-hydroxykynurenine (3-OHK), followed by the oxidative dimerization of 3-OHK to form an unstable intermediate, uncyclized xanthommatin (Uc-Xa). The intermediate Uc-Xa then rapidly cyclizes to form ommatins (Scheme 1). Although biological extracts have suggested the involvement of Uc-Xa, it has not been formally extracted or characterized from biological samples. Figon et al.[13] recently reinvestigated the ommochromes of housefly eyes and identified Xa, Dc-Xa, and Uc-Xa by combining the analytical tools, such as UV−vis and mass spectrometry with an artifact-free extraction protocol and subcellular fractionation of the ommochromes. This study supports the hypothesis that the synthesis of ommatin occurs in subcellular organelles and involves the dimerization of 3-OHK via intermediate Uc-Xa.

So far, only two approaches for synthesizing Xa have been reported in the literature. Both methods involve the oxidative dimerization of 3-OHK (Scheme 2a). The first method uses

https://doi.org/10.1021/jacsau.4c00667
JACS Au 2024, 4, 4307−4316

Scheme 2. Overview of the Previous and Current Work on Xa Synthesis

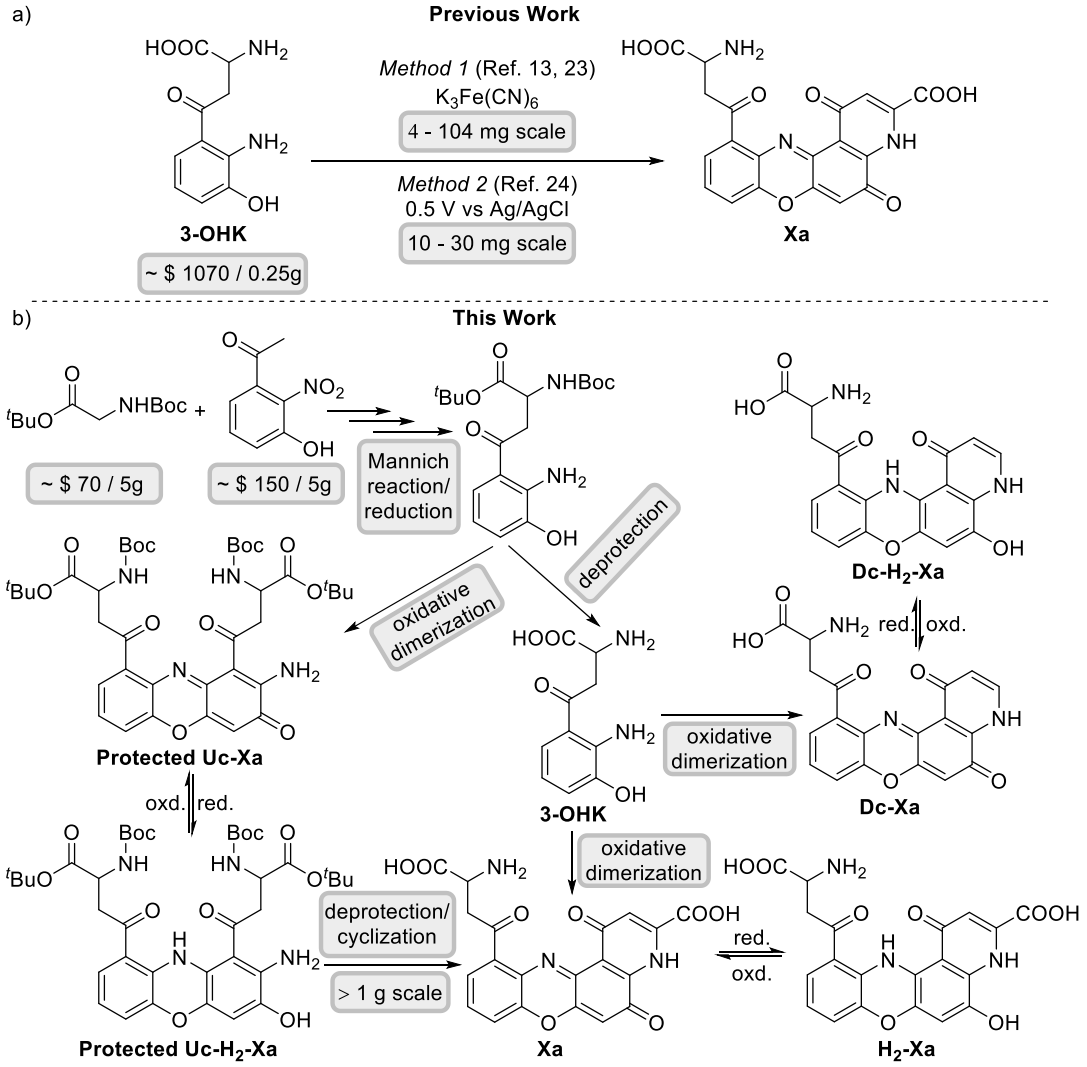

$K_3Fe(CN)_6$[13,23] as an oxidizing agent, while the second method employs electrocatalysis.[24] One of the limitations of the reported synthetic approaches is the high cost of the starting material, 3-OHK (~$1070 for 250 mg from Sigma-Aldrich). Additionally, the synthesis of Xa has been achieved only at the milligram scale (up to 100 mg). To further our efforts in natural product synthesis,[25−29] we designed a unique approach and completed a biomimetic total synthesis of Xa and protected Uc-Xa on a gram scale, using inexpensive and readily available starting materials (Scheme 2b). Furthermore, we have also synthesized Dc-Xa and Xa from a common intermediate using different oxidizing agents and proposed a possible mechanism for their formation. Our analysis using ^{1}H NMR, LC−MS, and HRMS analysis has shown that Xa and other biosynthetic precursors synthesized in this study exist in the equilibrium of oxidized and reduced forms (Xa/H_2-Xa, Dc-Xa/Dc-H_2-Xa, and protected Uc-Xa/Uc-H_2-Xa).

RESULTS AND DISCUSSION

Our research commenced by synthesizing a key compound **9** using the Mannich reaction as the main step (Scheme 3). First, commercially available, fully protected amino acid **1** was converted to bromo-derivative **2** (>10 g) using NBS and then treated with triethyl amine to generate imino derivative **3**. At the same time, TMS-enol ether **6** was synthesized by treating TBS-protected phenol **5** (synthesized from readily available phenol **4**) with LiHMDS and TMSCl. The Mannich reaction of in situ-formed imine **3** with freshly synthesized TMS-enol ether **6** in the presence of $TiCl_4$ yielded compound **7**, which without purification was treated with TBAF to give the nitrophenol **8** in 82% yield (>5 g) over three steps under optimized reaction conditions (see the Supporting Information, Table S1). Reduction of the nitro group of nitrophenol **8** with $B_2(OH)_4$ gave the key intermediate **9**, i.e., protected 3-OHK in 91% yield (>3.5 g). Subsequently, we used two approaches to synthesize Xa from protected 3-OHK **9**.

In the first approach, protected 3-OHK **9** was deprotected into 3-OHK **10** by treatment with TFA in a 90% yield. This was then subjected to oxidative dimerization using various oxidizing agents (Scheme 3 and Table 1). A trace amount of Xa **16** was observed in the presence of hemin (entry 2, Table 1) while using $K_3Fe(CN)_6$ (entry 3, Table 1); Xa **16** was formed in 30% yield. We observed that Xa was formed under alkaline conditions. On the other hand, Dc-Xa (**12**) was formed in the presence of $FeCl_3$/DDQ (entry 4, Table 1), PIFA (entry 6, Table 1), and $Mn(OAc)_3$ (entry 8, Table 1), with the reaction media being acidic. Importantly, ^{1}H NMR, LC−MS, and HRMS revealed that both Xa and Dc-Xa were

https://doi.org/10.1021/jacsau.4c00667
JACS Au 2024, 4, 4307−4316

Scheme 3. Synthesis of Ommatins—Xa/H_2-Xa, Dc-Xa/Dc-H_2-Xa, and Protected Uc-Xa/Uc-H_2-Xa

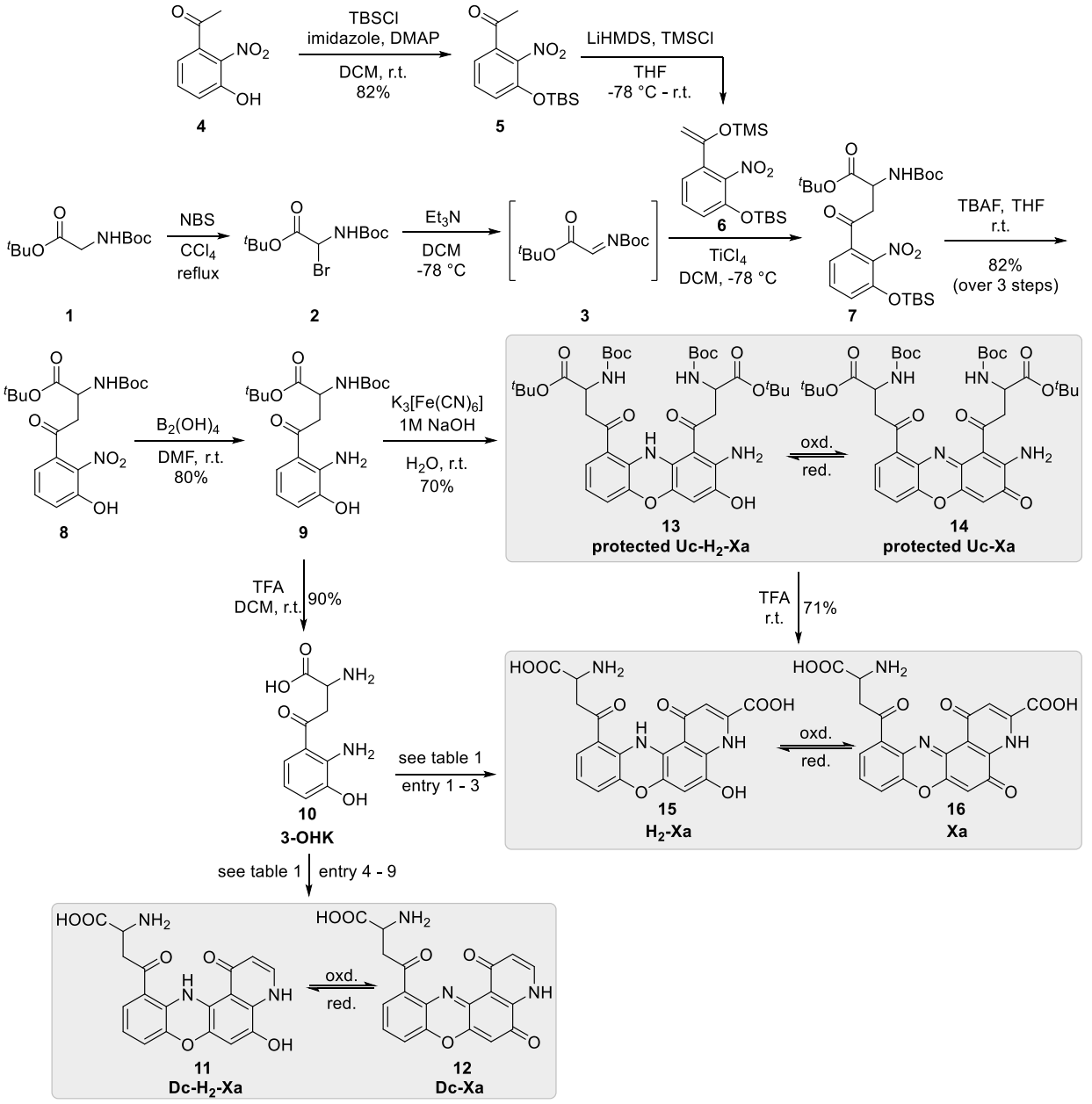

isolated as a mixture comprising oxidized and reduced forms as H_2-Xa/Xa (**15**/**16**) and Dc-H_2-Xa/Dc-Xa (**11**/**12**), respectively (see the Supporting Information, Experimental Section, for more detail). It is worth noting that ommitins are known to undergo autoredox reactions, which are highly sensitive to several factors, such as the pH, the type of solvent used, the presence or absence of light, and the availability of oxygen, which lead to varying compositions of the oxidized and reduced forms.[4,12,13] However, the conversion of **10** into Xa/H_2-Xa (entry 3, Table 1) or Dc-Xa/Dc-H_2-Xa (entry 8, Table 1) resulted in a low yield, probably due to the decomposition of intermediate products during the oxidative dimerization and final pyridone ring formation stages, which occur in one pot, and partly due to the difficulty in the purification step.

Consequently, a second approach was used to improve the product purity and yield and perform scale-up experiments. We began by performing oxidative dimerizations of protected 3-OHK **9** to obtain protected Uc-Xa (**14**), which was then purified by column chromatography before forming the final pyridone ring. The reaction was conducted on a scale of >3.5 g to yield over 2.5 g of Uc-Xa **14**, with a good yield of 70%. The product exists in reduced and oxidized forms as protected Uc-H_2-Xa/Uc-Xa (**13**/**14**) (Scheme 3) as determined by ^{1}H NMR and HRMS. In the final step, protected **13**/**14** was deprotected using TFA, during which it spontaneously underwent a cyclization−elimination−aromatization sequence to form H_2-Xa/Xa (**15**/**16**) in 71% isolated yield. Surprisingly, no Dc-H_2-Xa/Dc-Xa (**11**/**12**) was observed under the reaction condition despite the reaction being performed in neat TFA. This contrasts the literature, where it is speculated to undergo decarboxylation under acidic media.[4] These experimental results support the proposed biosynthetic pathway that oxidative dimerization occurs via the Uc-Xa intermediate and decarboxylation occurs during the oxidative dimerization step

https://doi.org/10.1021/jacsau.4c00667
JACS Au 2024, 4, 4307−4316

Table 1. Optimization of Oxidative Dimerization of 3-OHK

entry	reaction conditions	yield (%)[a]	
		11/12	15/16
1[b]	hemin (0.1 equiv), H_2O_2 (3 equiv), NaOH (5 equiv), CH_3CN/H_2O, r.t., 24 h		
2	hemin (2 equiv), NaOH (5 equiv), CH_3CN/H_2O, r.t., 24 h		trace
3	$K_3Fe(CN)_6$ (2.8 equiv), NaOH (1.7 equiv), H_2O, r.t., 2 h		30 (5:1)[c]
4	$FeCl_3$ (0.1 equiv), DDQ (1.2 equiv), CH_3CN, r.t., 16 h	10 (10:3)[c]	
5[b]	PIDA (1.2 equiv), CH_3CN, r.t., 16 h		
6	PIFA (1.2 equiv), CH_3CN, r.t., 16 h	15 (10:3)[c]	
7[b]	Ag_2O (2 equiv), CH_3CN, r.t., 16 h		
8	$Mn(OAc)_3 \cdot 2H_2O$ (1.2 equiv), CH_3CN, r.t., 16 h	30 (10:3)[c]	
9[d]	CAN (1.2 equiv), CH_3CN, r.t., 16 h		

[a]Isolated yield. [b]Starting material recovered. [c]Value in the parentheses is the ratio of reduced and oxidized forms. [d]Starting material decomposed.

before the final pyridone ring formation. Based on these experimental results, LC−MS analysis, and the literature reports, we proposed a probable mechanism for the formation of Xa/H_2-Xa and Dc-Xa/Dc-H_2-Xa under alkaline and acidic media, respectively, during the final oxidative dimerization/pyridone ring formation stage (Scheme 4).

The formation of Xa/H_2-Xa and Dc-Xa/Dc-H_2-Xa occurs through the intermediate Uc-Xa, a key compound in the proposed biosynthetic pathway of ommatins. The formation of this intermediate Uc-Xa was observed by monitoring the reaction using LC−MS analysis. The initial steps of the oxidative dimerization that lead to the formation of Uc-Xa are similar to those reported by Deravi's group.[24] During the LC−MS analysis, we observed m/z = 442.8, corresponding to $[M + H]^+$ of Uc-Xa, tautomerization of which results in the formation of intermediate **I**. Under alkaline conditions, **II** undergoes intramolecular cyclization to form a six-membered cyclic intermediate **III** that eliminates ammonia (NH_3) to form dihydro-pyridone intermediate **IV**. Finally, the oxidation of **IV** led to the formation of Xa, which can exist in both oxidized and reduced forms under the reaction conditions, as observed by LC−MS (m/z = 423.8 and 425.8 corresponding to $[M + H]^+$ of Xa and H_2-Xa, respectively). Under acidic conditions, with oxidizing agents such as PIFA or $FeCl_3$/DDQ or $Mn(OAc)_3$, the intermediate **V** underwent further oxidation, generating carboxyl radical **VI**.[30−32] Decarboxylation[31,33] of **VI** generated alkyl radical **VII**, which underwent further oxidation to form imine **VIII**. Tautomerization of imine to enamine led to ketoenamine **IX**, which can exist in equilibrium with intermediate **X**. Intramolecular cyclization of **X** followed by the elimination of ammonia from the resultant six-membered intermediate **XI** led to Dc-Xa formation. Like Xa, Dc-Xa also exists in the oxidized and reduced forms under the given reaction conditions, as observed by LC−MS (m/z = 379.8 and 381.8 corresponding to $[M + H]^+$ of Dc-Xa and Dc-H_2-Xa, respectively).

To determine the bandgap energies (E_g) of each synthesized ommatin (crude Xa, pure Xa, Uc-Xa, and Dc-Xa), Tauc plots were generated from their respective absorbance profiles (Figure 2a,b(i)). Tauc plots offer a methodical approach to analyze the optical absorption properties of materials and compute their energy bandgaps (Figure 2b(ii)). Despite their structural similarities, the pure Xa shows local absorption maxima of 280 and 470 nm, which is red-shifted compared to the crude (280 and 435 nm). Uc-Xa exhibits absorption maxima of 280 and 430 nm, while Dc-Xa shows the most blue-shifted maxima at 280 and 390 nm (Figure 2b(i)). From the absorbance spectra, the molar extinction coefficients were extrapolated for each compound in both UV and the visible wavelength regions. Within the UV region at 280 nm, the molar extinction coefficient was highest for Uc-Xa at 6641 ± 623 M^{-1} cm^{-1}, followed by pure Xa with a value of 4792 ± 86 M^{-1} cm^{-1}. However, the lowest molar extinction coefficient value was observed in Dc-Xa as 1000 ± 40 M^{-1} cm^{-1} (Table 2, Figure S1). Each compound also exhibited a different λ_{max} within the visible region due to its color variance in DMSO. Within the visible region, the molar extinction coefficient was highest for Uc-Xa at 430 nm with a value of 18,624 ± 308 M^{-1} cm^{-1}, followed by pure Xa at 470 nm with a molar extinction coefficient of 5446 ± 70 M^{-1} cm^{-1}, whereas the Dc-Xa compound had a strong absorption peak at 390 nm with a molar extinction coefficient of 1342 ± 73 M^{-1} cm^{-1}. When taken together, these data indicate that Dc-Xa is the weakest light absorber within these regions. Such differences might account for why the crude Xa is also blue-shifted relative to the purified Xa, suggesting that the crude may include Dc-Xa.

These absorption peaks are indicative of unique structures and electronic transitions embedded within each compound. Based on these values, we extrapolated relative bandgap energies for each compound using Tauc plots similar to previous reports. Based on these calculations, we can infer the direct energy bandgap in two linear segments (Figure 2b(ii)). The first transition at lower energy signifies the optical gap, corresponding to the onset of optical absorption and the creation of an electron−hole pair. The second transition represents the fundamental energy gap, which is the energy difference between the valence band (lowest unoccupied molecular orbitals, LUMOs) and the conduction band (highest occupied molecular orbitals, HOMOs).[34] Based on these analyses, the pure Xa and Dc-Xa exhibited similar energy bandgaps calculated as 3.85 and 3.83 eV, respectively. Crude Xa showed the lowest energy bandgap of 3.76 eV, while Uc-Xa exhibited the widest energy bandgap of 3.97 eV. Based on the absorption spectra, Uc-Xa demonstrated a greater degree of intramolecular charge transfer, as evidenced by its blue-shifted spectra relative to pure Xa.

We next recorded cyclic voltammograms of each material to better understand its HOMO and LUMO energies. Not surprisingly, each compound demonstrated reversible redox behavior with peaks between −0.2 and 0.6 V (Figure 2c). HOMO and LUMO energy levels were then obtained from these cyclic voltammograms. Crude Xa exhibited HOMO/LUMO levels of −1.40/−5.16 eV, which agreed well with previous reports.[35] This differed slightly from that of pure Xa, Uc-Xa, and Dc-Xa, which had HOMO/LUMO levels of −1.32/−5.17, −1.19/−5.16, and −1.35/−5.18 eV, respectively (Figure 2d). Based on the energy bandgap calculation, both pure Xa and Dc-Xa demonstrated similar HOMO and LUMO energy levels. This observation implies a strong similarity between these compounds, both of which are derived from hydroxykynurenine. The higher energy levels of Uc-Xa are likely attributed to the extra conjugation of double bonds that increase the energy of HOMO.

https://doi.org/10.1021/jacsau.4c00667
JACS Au 2024, 4, 4307−4316

Scheme 4. Plausible Mechanism—(a) Oxidative Dimerization of 3-OHK to Uc-Xa; (b) Formation of Xa/H_2-Xa under Alkaline Reaction Condition; and (c) Formation of Dc-Xa/Dc-H_2-Xa under Acidic Reaction Condition

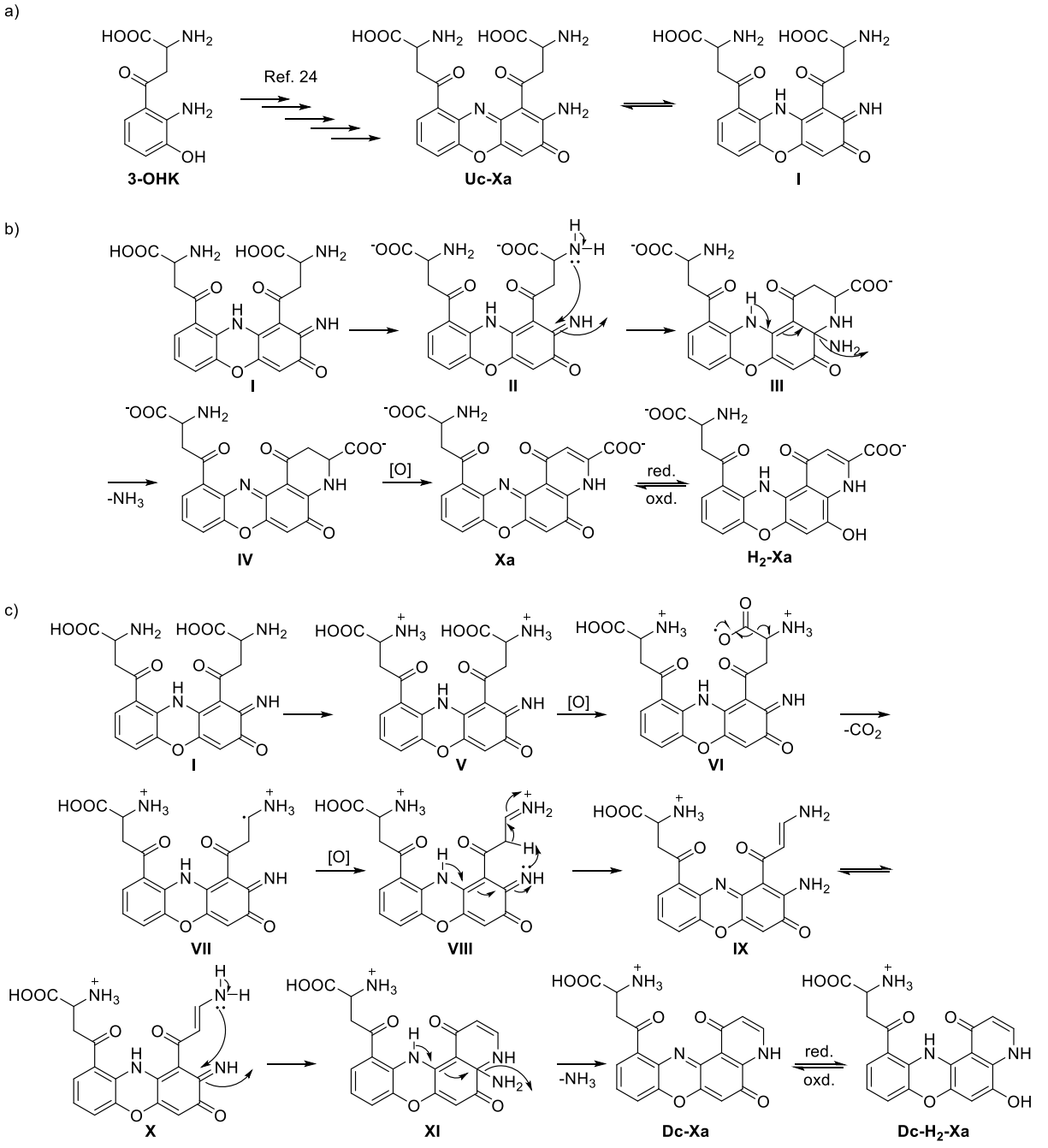

To further explore the functional properties of each compound, we next explored their antioxidant capacities by using an oxygen radical antioxidant capacity (ORAC) activity assay. Xa is known to exhibit antioxidant behavior,[36,37] so we wanted to investigate how compound purity and functionality contributed to this function. Each compound was compared to an antioxidant standard, Trolox, which is a water-soluble analogue of vitamin E (Figure S2). When comparing 5 μM concentrations of Trolox to 5 μM of each sample, we observed that Uc-Xa exhibited the lowest antioxidant capabilities with a net area under the curve (AUC) of 0.059 ± 0.005 compared to Trolox which had a net AUC of 0.535 ± 0.038 (Figure 3). This differed from the crude Xa, pure Xa, and Dc-Xa, which had net AUC values of 0.675 ± 0.124, 0.627 ± 0.109, and 1.825 ± 0.139, respectively. From these data, it appears that the loss of the carboxylic acid significantly enhances the ability of these compounds to quench reactive oxygen species. We suspect that the loss of the carboxylic acid group is increasing the ability of the molecules to donate electrons which may ultimately enhance their free radical scavenging ability similar to past reports.[38]

CONCLUSIONS

We have developed a novel, bioinspired method for synthesizing ommatins from a common intermediate compound, protected 3-OHK. The main building block (protected 3-OHK) was synthesized using the Mannich reaction as the key step and then converted into the ommatin scaffold through a

https://doi.org/10.1021/jacsau.4c00667
JACS Au 2024, 4, 4307−4316

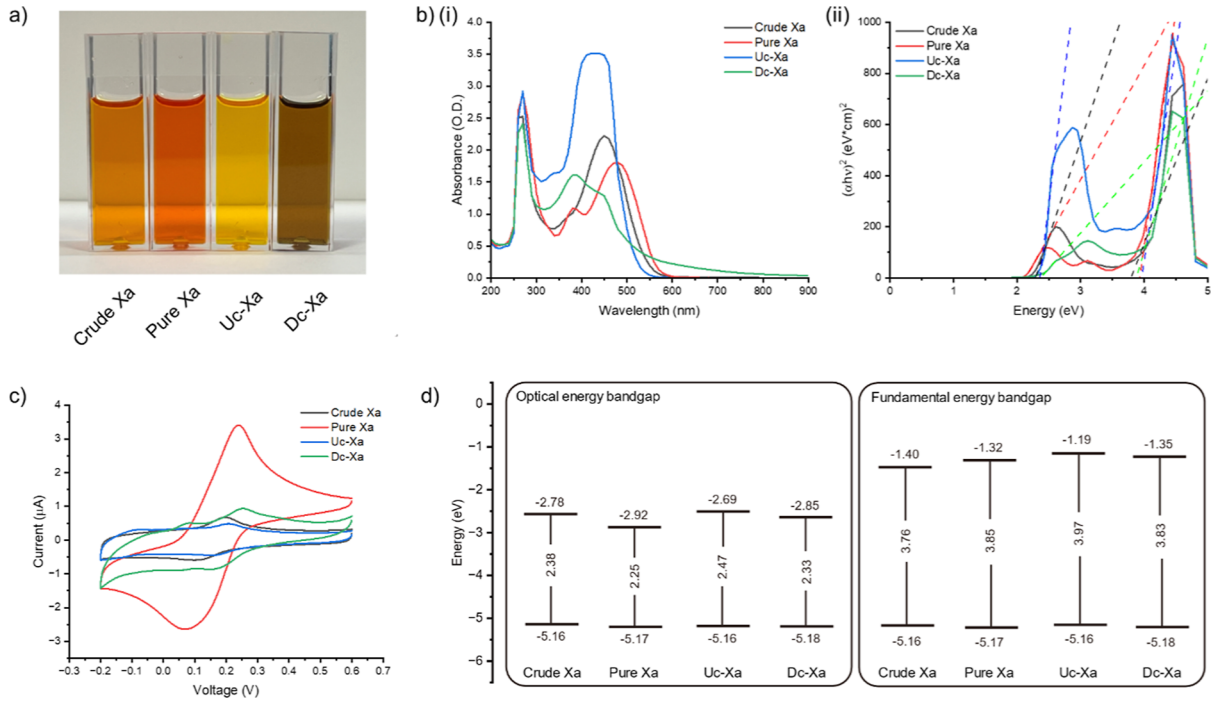

Figure 2. Analysis of optoelectronic properties. (a) Image of crude Xa, pure Xa, Uc-Xa, and Dc-Xa at 1.5 mM in DMSO. (b) Comparison of (i) absorbance spectra of each solution and (ii) their direct energy bandgap as extrapolated via a Tauc plot. (c) Electrochemical analysis of generated CV curves of ommatins in DMSO containing 0.1 M lithium triflate collected at a 50 mV s^{-1} scanning speed. (d) Comparison of the energy band alignments as extrapolated from the optical and electrochemical measurements.

Table 2. Molar Extinction Coefficients (ε) of Ommatins—Pure Xa, Uc-Xa, and Dc-Xa Dissolved in DMSO[a]

compound	ε (M^{-1} cm^{-1}) at λ_{280nm}	ε (M^{-1} cm^{-1}) at λ_{max}
pure Xa	4792 ± 86	5446 ± 70 at 470 nm
Uc-Xa	6641 ± 623	18,624 ± 308 at 430 nm
Dc-Xa	1000 ± 40	1342 ± 73 at 390 nm

[a]Values reported are an average for three replicates, including standard deviation.

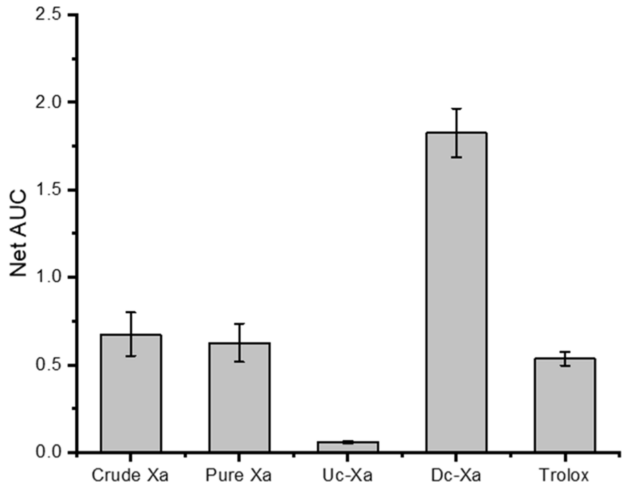

Figure 3. Net AUC of a 5 μM solution of each sample (crude Xa, pure Xa, Uc-Xa, and Dc-Xa) in 0.1 M PBS, pH 7.2 compared to a 5 μM Trolox standard as measured by the ORAC activity assay. The net AUC was calculated by subtracting the AUC of the blank (0 μM Trolox and 0.1 M PBS) from the AUC of the measured sample. Values reported are an average for three replicates, including standard deviation.

one-pot oxidative dimerization−cyclization process. We observed the formation of Xa/H_2-Xa when the reaction medium was alkaline and Dc-Xa/Dc-H_2-Xa when the oxidizing agent was acidic during the oxidative dimerization of 3-OHK. We proposed a possible mechanism for the formation of Xa/H_2-Xa in alkaline conditions and Dc-Xa/Dc-H_2-Xa under acidic conditions based on our analysis and existing literature. Additionally, we sequentially synthesized Xa/H_2-Xa by first synthesizing an essential biosynthetic precursor, Uc-Xa/Uc-H_2-Xa, through the oxidative dimerization of protected 3-OHK, followed by deprotection and intramolecular cyclization. All synthesized ommatins were meticulously characterized using a range of spectroscopic techniques, including UV−vis, FTIR, NMR, LC−MS, and HRMS. We observed that they exist in a dynamic equilibrium between oxidized and reduced forms under the reaction condition. Our ability to scale up the synthesis of Xa/H_2-Xa to over 1 g using this new approach, with an overall yield of 27%, is a testament to the robustness of our method. We also successfully synthesized protected Uc-Xa/Uc-H_2-Xa and Dc-Xa/Dc-H_2-Xa, providing further support for the proposed biosynthetic pathway in which ommatins are produced via a key biosynthetic precursor, Uc-Xa.

The absorption spectra of Xa, Dc-Xa, and Uc-Xa displayed distinct optical signatures (λ_{max}) in the visible region, resulting in varied coloration in DMSO. The molar extinction coefficient was highest for Uc-Xa at 430 nm, followed by pure Xa at 470 nm and Dc-Xa at 390 nm. The optical and fundamental energy bandgap was determined using a Tauc plot and CV, revealing that Xa had the narrowest gap, and Uc-Xa had the widest gap. In addition, we assessed the antioxidant activity of the synthesized ommatins using an ORAC activity test, and the results were highly encouraging, with the Dc-Xa significantly enhancing the ability to quench reactive oxygen species in comparison to the positive control Trolox used in this study.

https://doi.org/10.1021/jacsau.4c00667
JACS Au 2024, 4, 4307−4316

The Xa showed activity like Trolox, while Uc-Xa displayed the lowest activity. These compelling findings indicate promising prospects for developing antioxidant compounds with potential pharmaceutical applications, instilling optimism for the future widespread use of biomimetic compounds.

MATERIALS AND METHODS

Detailed information on the synthetic procedure, compound characterization data, other experimental procedures (UV−vis spectroscopy and the ORAC activity assay), copies of ^{1}H and ^{13}C NMR, and HRMS spectra is provided in the Supporting Information file.

Synthetic Procedure and Compound Characterization

All reagents and solvents were obtained from Fisher Scientific, Sigma-Aldrich, or TCI and used without further purification. Tetrahydrofuran (THF) was distilled from benzophenone and sodium metal under a positive-pressure argon atmosphere immediately before use. All other anhydrous solvents were purchased from VWR. Analytical thin layer chromatography (TLC) was performed on silica gel 60 F_{254} precoated plates (0.25 mm) from EMD Millipore Corp., and components were visualized by ultraviolet light (254 nm) and TLC staining solutions (phosphomolybdic acid (PMA), $KMnO_4$, or a solution of $Ce(SO_4)_2$/ammonium phosphomolybdate/10% H_2SO_4 followed by heating). Reported R_f values were determined for TLC. EMD silica gel 60 (particle size 40−63 μm) 230−400 mesh was used for column chromatography. ^{1}H NMR spectra were recorded at ambient temperature on a 500 MHz Bruker NMR spectrometer in the indicated solvent. All ^{1}H NMR experiments are reported in δ units, parts per million (ppm) downfield of TMS and were measured relative to the signals for chloroform (7.26 ppm), methanol (3.31 ppm), and dimethylsulfoxide (2.50 ppm). Data for ^{1}H NMR are reported as follows: chemical shift (δ ppm), multiplicity (s = singlet, d = doublet, t = triplet, q = quartet, m = multiplet), integration, and coupling constant (Hz), whereas ^{13}C NMR analyses are reported in terms of chemical shift. NMR data was analyzed by using MestReNova Software ver. 12.0.3-21384. LC−MS was performed on an Agilent 1260 Infinity LC instrument coupled to an Agilent 6120 single quadrupole mass spectrometer with electrospray ionization. FTIR spectra were performed on a Bruker alpha platinum ATR. High-resolution mass spectra were obtained on a Q-Exactive Orbitrap (Thermo Fisher Scientific) using a syringe pump with direct infusion. Detailed information about the reaction conditions, experimental procedures, and characterization of all newly synthesized compounds is available in the Supporting Information.

UV−Vis Spectroscopy

UV−vis absorption of synthesized ommatins was performed on a SpectraMax M5 spectrophotometer. Detailed experimental procedures, molar extinction coefficient calculation, and UV−vis spectra are available in the Supporting Information.

Electrochemical Analysis

All cyclic voltammograms were collected using a Gamry Interface 1000 B potentiostat with a three-electrode system comprising a glassy carbon working electrode, platinum wire counter electrode, and a silver−silver chloride (Ag/AgCl with saturated KCl) reference electrode. The supporting electrolyte consisted of 3.0 mL of DMSO containing 0.1 M lithium triflate (LiOTf, Sigma-Aldrich). Voltammograms were scanned over five cycles from −0.2 to 0.6 V at a scanning speed of 50 mV s^{-1}.

Oxygen Radical Antioxidant Capacity Activity Assay

A detailed experimental procedure for the ORAC activity assay and the net AUC calculations are available in the Supporting Information.

ASSOCIATED CONTENT

Supporting Information

The Supporting Information is available free of charge at https://pubs.acs.org/doi/10.1021/jacsau.4c00667.

Synthetic procedures and compound characterization, UV−vis spectroscopy, ORAC activity assay, references, and copies of ^{1}H, ^{13}C NMR and HRMS spectra (PDF)

AUTHOR INFORMATION

Corresponding Authors

Prakash T. Parvatkar − *Department of Chemistry and Chemical Biology, Northeastern University, Boston, Massachusetts 02115, United States;* orcid.org/0000-0002-9695-767X; Email: p.parvatkar@northeastern.edu

Roman Manetsch − *Department of Chemistry and Chemical Biology, Northeastern University, Boston, Massachusetts 02115, United States; Department of Pharmaceutical Sciences, Center for Drug Discovery, and Barnett Institute of Chemical and Biological Analysis, Northeastern University, Boston, Massachusetts 02115, United States;* orcid.org/0000-0001-7038-6867; Phone: +1-6173736316; Email: r.manetsch@northeastern.edu; Fax: +1-6173738795

Authors

Lili Huang − *Department of Chemistry and Chemical Biology, Northeastern University, Boston, Massachusetts 02115, United States*

Taehwan Kim − *Department of Chemistry and Chemical Biology, Northeastern University, Boston, Massachusetts 02115, United States*

Olivia J. Armendarez − *Department of Chemistry and Chemical Biology, Northeastern University, Boston, Massachusetts 02115, United States*

Leila F. Deravi − *Department of Chemistry and Chemical Biology, Northeastern University, Boston, Massachusetts 02115, United States;* orcid.org/0000-0003-3226-2470

Complete contact information is available at: https://pubs.acs.org/10.1021/jacsau.4c00667

Author Contributions

PTP and RM proposed the synthesis, designed the experiments, and supervised. LH performed the chemical synthesis experiments. LH, PTP, and RM characterized all compounds. LFD, TK, and OJA studied the optoelectronic properties and antioxidant activity. PTP wrote the manuscript with the help of all authors. All authors have approved the final version of the manuscript. CRediT: **Lili Huang** formal analysis, investigation, methodology; **Taehwan Kim** investigation, methodology; **Olivia J. Armendarez** methodology; **Leila F Deravi** resources, supervision, writing - review & editing; **Prakash T. Parvatkar** conceptualization, data curation, formal analysis, investigation, methodology, supervision, validation, visualization, writing - original draft, writing - review & editing; **Roman Manetsch** conceptualization, data curation, funding acquisition, resources, supervision, validation, writing - review & editing.

Funding

This work was supported in part by the Office of Naval Research (Award N00014-22-1-2053; LFD, TK, OJA).

Notes

The authors declare no competing financial interest.

■ ACKNOWLEDGMENTS

The authors express gratitude for the staffing and instrumentation support provided by the Northeastern University NMR Core Facility. This work utilized an NMR spectrometer purchased with funding from a National Institutes of Health SIG grant (S10OD032452).

■ REFERENCES

(1) Butenandt, A.; Schafer, W. Ommochromes. In *Recent Progress in the Chemistry of Natural and Synthetic Coloring Matters and Related Fields*; Gore, T. S., Ed.; Academic Press: New York, 1962; pp 13−62.
(2) Dontsov, A. E.; Ushakova, N. A.; Sadykova, V. S.; Bastrakov, A. I. Ommochromes from Hermetia illucens: Isolation and Study of Antioxidant Characteristics and Antimicrobial Activity. *Appl. Biochem. Microbiol.* **2020**, *56* (1), 91−95.
(3) Williams, T. L.; DiBona, C. W.; Dinneen, S. R.; Jones Labadie, S. F.; Chu, F. X.; Deravi, L. F. Contributions of Phenoxazone-Based Pigments to the Structure and Function of Nanostructured Granules in Squid Chromatophores. *Langmuir* **2016**, *32* (15), 3754−3759.
(4) Figon, F.; Casas, J. Ommochromes in invertebrates: biochemistry and cell biology. *Biol. Rev.* **2019**, *94* (1), 156−183.
(5) Bolognese, A.; Correale, G.; Manfra, M.; Lavecchia, A.; Mazzoni, O.; Novellino, E.; Barone, V.; Pani, A.; Tramontano, E.; La Colla, P.; Murgioni, C.; Serra, I.; Setzu, G.; Loddo, R. Antitumor agents.: 1.: Synthesis, biological evaluation, and molecular modeling of 5-pyrido[3,2-]phenoxazin-5-one, a compound with potent antiproliferative activity. *J. Med. Chem.* **2002**, *45* (24), 5205−5216.
(6) Kumar, A.; Williams, T. L.; Martin, C. A.; Figueroa-Navedo, A. M.; Deravi, L. F. Xanthommatin-Based Electrochromic Displays Inspired by Nature. *ACS Appl. Mater. Interfaces* **2018**, *10* (49), 43177−43183.
(7) Becker, E. Über die Natur des Augenpigments von Ephestia kuhniella und seinen vergleich mit den Aaugenpigmenten anderer insekten. *Biol. Zentralbl.* **1939**, *59*, 597−627.
(8) Becker, E. Über eigenschaften, verbreitung und die genetischentwicklungs-physiologische bedeutung der pigmente der ommatin-und ommingruppe (ommochrome) bei den arthropoden. *Mol. Gen. Genet.* **1942**, *80*, 157−204.
(9) Linzen, B. The Tryptophan → Ommochrome Pathway in Insects. *Adv. Insect Physiol.* **1974**, *10*, 117−246.
(10) Needham, A. E. *The Significance of Zoochromes*; Springer-Verlag: Berlin, Germany, 1974; p 452.
(11) Bolognese, A.; Liberatore, R. Photochemistry of Ommochrome Pigments. *J. Heterocycl. Chem.* **1988**, *25* (4), 1243−1246.
(12) Cordell, G. A.; Daley, S. K. Biosynthesis of the Ommochromes and Papiliochromes. *Rec. Nat. Prod.* **2021**, *15* (6), 420−432.
(13) Figon, F.; Munsch, T.; Croix, C.; Viaud-Massuard, M. C.; Lanoue, A.; Casas, J. Uncyclized xanthommatin is a key ommochrome intermediate in invertebrate coloration. *Insect Biochem. Mol. Biol.* **2020**, *124*, 103403.
(14) Lewis, L. L. M.; Dörschmann, P.; Seeba, C.; Thalenhorst, T.; Roider, J.; Iloki Assanga, S. B.; Ruiz, J. C. G.; Del Castillo Castro, T.; Rosas-Burgos, E. C.; Plascencia-Jatomea, M.; Ezquerra Brauer, J. M.; Klettner, A. Properties of Cephalopod Skin Ommochromes to Inhibit Free Radicals, and the Maillard Reaction and Retino-Protective Mechanisms in Cellular Models Concerning Oxidative Stress, Angiogenesis, and Inflammation. *Antioxidants* **2022**, *11* (8), 1574.
(15) Riddiford, L. M.; Ajami, A. M. Identification of an ommochrome in the eyes and nervous systems of saturniid moths. *Biochemistry* **1971**, *10*, 1451−1455.
(16) Butenandt, A.; Schiedt, U.; Biekert, E.; Cromartie, R. J. T. Über Ommochrome, IV. Mitteilung: Konstitution des Xanthommatins. *Justus Liebigs Ann. Chem.* **1954**, *590*, 75−90.
(17) Futahashi, R.; Kurita, R.; Mano, H.; Fukatsu, T. Redox alters yellow dragonflies into red. *Proc. Natl. Acad. Sci. U.S.A.* **2012**, *109* (31), 12626−12631.
(18) Langer, H. Properties and functions of screening pigments in insect eyes. In *Photoreceptor Optics*; Springer: Berlin, Heidelberg, 1975; pp 429−455.
(19) Horowitz, N. H.; Baumberger, J. P. Studies on the respiratory pigment of Urechis eggs. *J. Biol. Chem.* **1941**, *141*, 407−415.
(20) Linzen, B. Über Ommochrome, XVI Über die Identifizierung des "Urechochroms" als Xanthommatin. *Biol. Chem.* **1959**, *314*, 12−14.
(21) Linzen, B.; Bückmann, D. Biochemische und histologische Untersuchungen zur Umfärbung der Raupe von Cerura vinula L. *Z. Naturforsch., B: J. Chem. Sci.* **1961**, *16*, 6−18.
(22) Harano, T.; Chino, H. A new diaphorase from Bombyx silkworm eggs—cytochrome c reductase activity mediated with xanthommatin. *Arch. Biochem. Biophys.* **1971**, *146*, 467−476.
(23) Butenandt, A.; Schiedt, U.; Biekert, E. Uber Ommochrome, III. Mitteilung: synthese des Xanthommatins. *Adv. Cycloaddit.* **1954**, *588*, 106−116.
(24) Williams, T. L.; Lopez, S. A.; Deravi, L. F. A Sustainable Route To Synthesize the Xanthommatin Biochrome via an Electro-catalyzed Oxidation of Tryptophan Metabolites. *ACS Sustain. Chem. Eng.* **2019**, *7* (9), 8979−8985.
(25) Dowgiallo, M. G.; Miller, B. C.; Kassu, M.; Smith, K. P.; Fetigan, A. D.; Guo, J. J.; Kirby, J. E.; Manetsch, R. The convergent total synthesis and antibacterial profile of the natural product streptothricin F. *Chem. Sci.* **2022**, *13* (12), 3447−3453.
(26) Parvatkar, P. T.; Smotkin, E. S.; Manetsch, R. Total synthesis of (±)-decursivine via BINOL-phosphoric acid catalyzed tandem oxidative cyclization. *Sci. Rep.* **2021**, *11* (1), 19915.
(27) Parvatkar, P. T.; Majik, M. S. Microwave-assisted reductive cyclization: an easy entry to the indoloquinolines and spiro[2H-indole-2,3′-oxindole]. *RSC Adv.* **2014**, *4* (43), 22481−22486.
(28) Volvoikar, P. S.; Parvatkar, P. T.; Tilve, S. G. Tandem Reductive Cyclization-Dehydration Approach for the Synthesis of Cryptolepine Hydroiodide and Its Analogues. *Eur. J. Org Chem.* **2013**, *2013* (11), 2172−2178.
(29) Parvatkar, P. T.; Tilve, S. G. An efficient synthesis of indoloquinoline alkaloid - neocryptolepine (cryptotackieine). *Tetrahedron Lett.* **2011**, *52* (49), 6594−6596.
(30) Boto, A.; Hernández, R.; Suárez, E. Tandem radical decarboxylation-oxidation of amino acids:: A mild and efficient method for the generation of *N*-acyliminium ions and their nucleophilic trapping. *J. Org. Chem.* **2000**, *65* (16), 4930−4937.
(31) Kiyokawa, K.; Yahata, S.; Kojima, T.; Minakata, S. Hypervalent Iodine(III)-Mediated Oxidative Decarboxylation of *β*,*γ*-Unsaturated Carboxylic Acids. *Org. Lett.* **2014**, *16* (17), 4646−4649.
(32) Snider, B. B. Mechanisms of Mn(OAc)3-based oxidative free-radical additions and cyclizations. *Tetrahedron* **2009**, *65* (52), 10738−10744.
(33) Wang, H.; Fan, R. H. Stereoselective Synthesis of 2-Carbamoyl-2-cyanocyclopropanecarboxylates by Tandem Oxidative Cyclization and Neighboring Group-Assisted Decarboxylation. *J. Org. Chem.* **2010**, *75* (20), 6994−6997.
(34) Dongol, M.; El-Nahass, M. M.; El-Denglawey, A.; Elhady, A. F.; Abuelwafa, A. A. Optical Properties of Nano 5,10,15,20-Tetraphenyl-21H,23H-Prophyrin Nickel (II) Thin Films. *Curr. Appl. Phys.* **2012**, *12* (4), 1178−1184.
(35) Martin, C. L.; Flynn, K. R.; Kim, T.; Nikolic, S. K.; Deravi, L. F.; Wilson, D. J. Color-Changing Paints Enabled by Photoresponsive Combinations of Bio-Inspired Colorants and Semiconductors. *Adv. Sci.* **2023**, *10* (32), No. e2302652, DOI: 10.1002/advs.202302652.
(36) Martin, C. A.; Rezaeeyazdi, M.; Colombani, T.; Dinneen, S. R.; Kumar, A.; Bencherif, S. A.; Deravi, L. F. A bioinspired, photostable UV-filter that protects mammalian cells against UV-induced cellular damage. *Chem. Commun.* **2019**, *55* (80), 12036−12039.
(37) Martin, C. L.; Flynn, K. R.; Kim, T.; Nikolic, S. K.; Deravi, L. F.; Wilson, D. J. Color-Changing Paints Enabled by Photoresponsive

Combinations of Bio-Inspired Colorants and Semiconductors. *Adv. Sci.* **2023**, *10* (32), No. e2302652.
(38) Zhang, J.; Li, L.; Wang, X.; Wang, Z.; Zheng, C.; Zhang, H.; Wang, H.; Li, P.; Zhai, X.; Li, H. Inhibitory mechanism against oxidative stress and biological activities of canolol. *Acta Polym. Pharm.-Drug Res.* **2017**, *74*, 25−29.

https://doi.org/10.1021/jacsau.4c00667
JACS Au 2024, 4, 4307−4316